Supporting Information for

Interface-assisted phase transition in MOF-derived MoS_2/CoS_2 heterostructures for highly efficient dual-pH hydrogen evolution and overall water splitting

Pu Chang,[1] Tian Wang,[2] Zongli Liu,[1] Xiaohu Wang,[3] Jiatong Zhang,[1] Hongfei Xiao,[1] Lixiu Guan,[2,] and Junguang Tao[1,*]*

[1]School of Materials Science and Engineering, Hebei University of Technology, Tianjin 300132, China

[2]School of Science, Hebei University of Technology, Tianjin 300401, China

[3]Rising Graphite Applied Technology Research Institute, Chinese Graphite Industrial Park-Xinghe, Ulanqab, Inner Mongolia, 013650, China

Material Synthesis:

Synthesis of cobalt-based metal-organic framework (Co-MOF) nanoarrays on carbon cloth (CC): CC was immersed in acetone, ethanol, and deionized (DI) water for ultrasonically cleaning of 30 min in each step.

Firstly, 0.55 g $Co(NO_3)_2 \cdot 6H_2O$ and 1.30 g 2-methylimidazole ($C_4H_6N_2$) were uniformly dissolved in 40 mL water. Subsequently, a piece of treated CC (2×3 cm^2) was immersed in the above solution at room temperature for 5 h. Finally, the obtained purple CC after the reaction was rinsed with ethanol repeatedly and dried overnight to obtain Co-MOF/CC.

Synthesis of $CoMoO_4$ on CC: The prepared Co-MOF/CC was immersed into 50 mL solution (ethanol: DI water = 3:2) containing 0.91 g sodium molybdate (Na_2MoO_4) and kept at 100 °C for 3 h. After etching, the

samples were washed by ethanol and dried overnight to obtain $CoMoO_4$/CC.

Synthesis of 1T-2H MoS_2/CoS_2 heterostructure on CC: The 1T-2H MoS_2/CoS_2 heterostructure was prepared by simple one-step calcination at 400 °C for 5 h under Ar atmosphere, where 1 g thiourea powder and $CoMoO_4$/CC precursors were placed in the upstream and downstream positions in the tube furnace, respectively. For comparison, different etching time of 1 h, 3 h and 5 h were used without changing the other conditions. The mass loadings of all samples on CC are given in Table S1.

Synthesis of CoS_2 on CC: The conditions remained the same as in the preparation of $CoMoO_4$ step except for the replacement of 0.91 g sodium molybdate with 0.69 g $Co(NO_3)_2 \cdot 6H_2O$.

Synthesis of MoS_2 on CC: The MoS_2 was prepared on CC using a simple hydrothermal method. A piece of treated CC (2×3 cm^2) substrate was immersed in 40 mL aqueous solution composed of 0.25 g Na_2MoO_4 and 0.5 g TAA. Subsequently, the solution was transferred into a 50 mL Teflon-lined stainless autoclave and heated to 200° for 20 h. The prepared sample was washed with ethanol and dried at 60° to obtain the MoS_2 on CC.

Preparation of Pt/C and IrO_2 on CC: The commercial Pt/C (20 wt%, Aladdin) and IrO_2 (99%, Aladdin) was drop-casted on CC using catalyst ink. The catalyst ink was obtained by dispersing Pt/C and IrO_2 uniformly in a solution containing 0.5 mL ethanol and 50 μL Nafion, respectively.

The mass loading of Pt/C was calculated to be ~2.0 mg cm^{-2}.

Turnover frequency (TOF) calculations for HER and OER:

The TOF (s^{-1}) of HER and OER are calculated according to the following equations (1) and (2), respectively.

$$TOF = \frac{|J|S_{geo}}{2Fn} \quad (1)$$

$$TOF = \frac{|J|S_{geo}}{4Fn} \quad (2)$$

where J is the measured current density (A cm^{-2}), S_{geo} is geometric area of the working electrode (1 cm^2), F is the Faraday constant (96485 C mol^{-1}), and n is the mole number of the active site of the electrode.[1, 2]

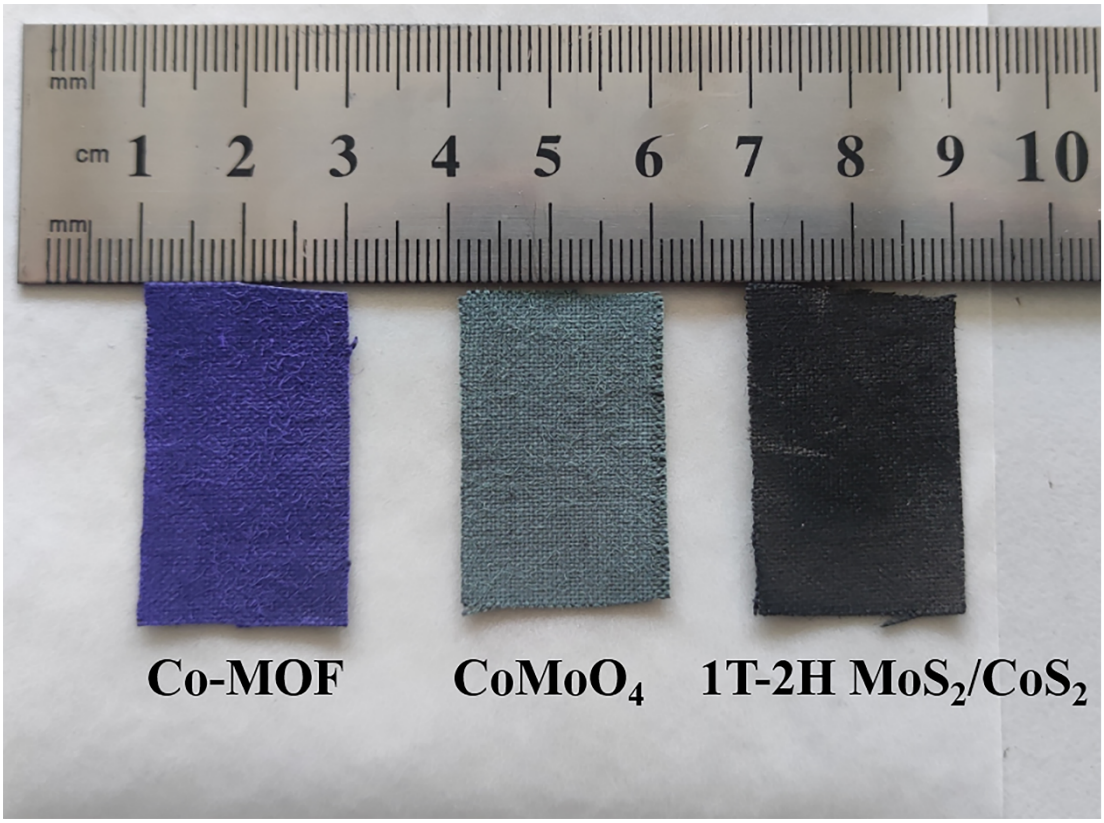

Fig. S1. Optical pictures of (from left to right) Co-MOF, $CoMoO_4$, and 1T-2H MoS_2/CoS_2.

Co-MOF nanoarrays are grown directly on CC by the reaction of cobaltous nitrate hexahydrate with 2-methylimidazole in aqueous solution at room temperature. As shown in Fig. S2(a), the XRD results confirm the formation of Co-MOF precursor. Then, the obtained uniform Co-MOF nanoarrays reacted with sodium molybdate (Na_2MoO_4) solution at 100 °C for 3 h *via* ion-exchange and the etching process to generate porous $CoMoO_4$ nanoarrays according to：

$$Co^{2+} + MoO_4^{2-} \rightarrow CoMoO_4$$

The corresponding XRD pattern [see Fig. S2(b)] is clearly attributed to the $CoMoO_4$.

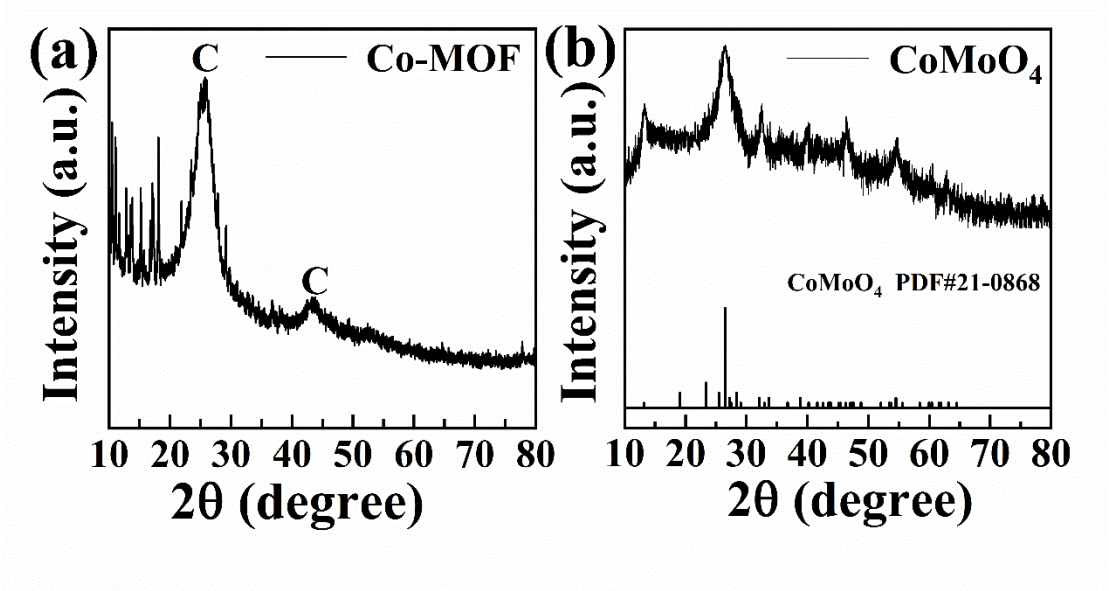

Fig. S2. XRD patterns of precursors Co-MOF (a) and $CoMoO_4$ (b). The peak labeled C is attributed to the carbon cloth.

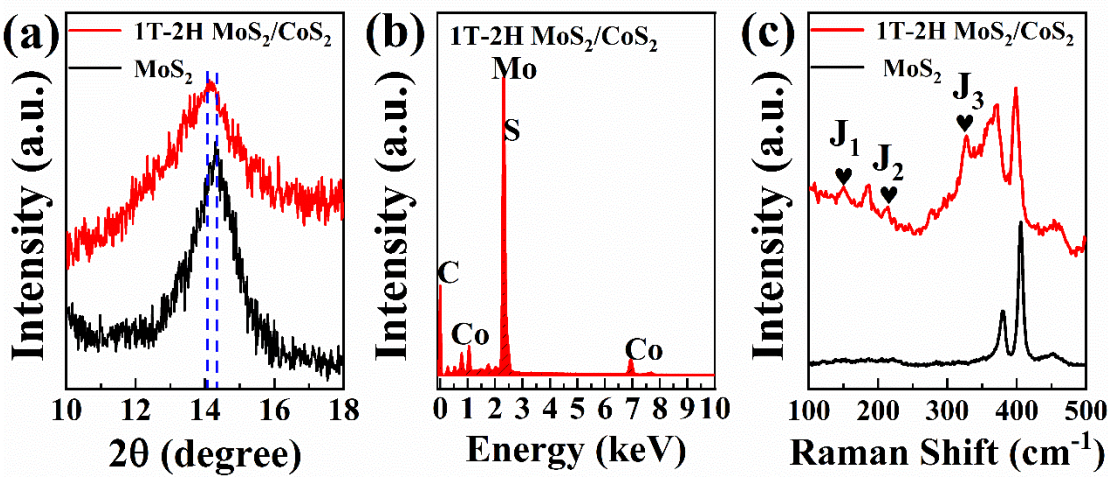

Fig. S3. (a) XRD patterns of 1T-2H MoS_2/CoS_2 and pure MoS_2 from the selected range in Fig. 1(b). (b) EDS analysis of 1T-2H MoS_2/CoS_2. (c) Raman spectra of 1T-2H MoS_2/CoS_2 and pure MoS_2.

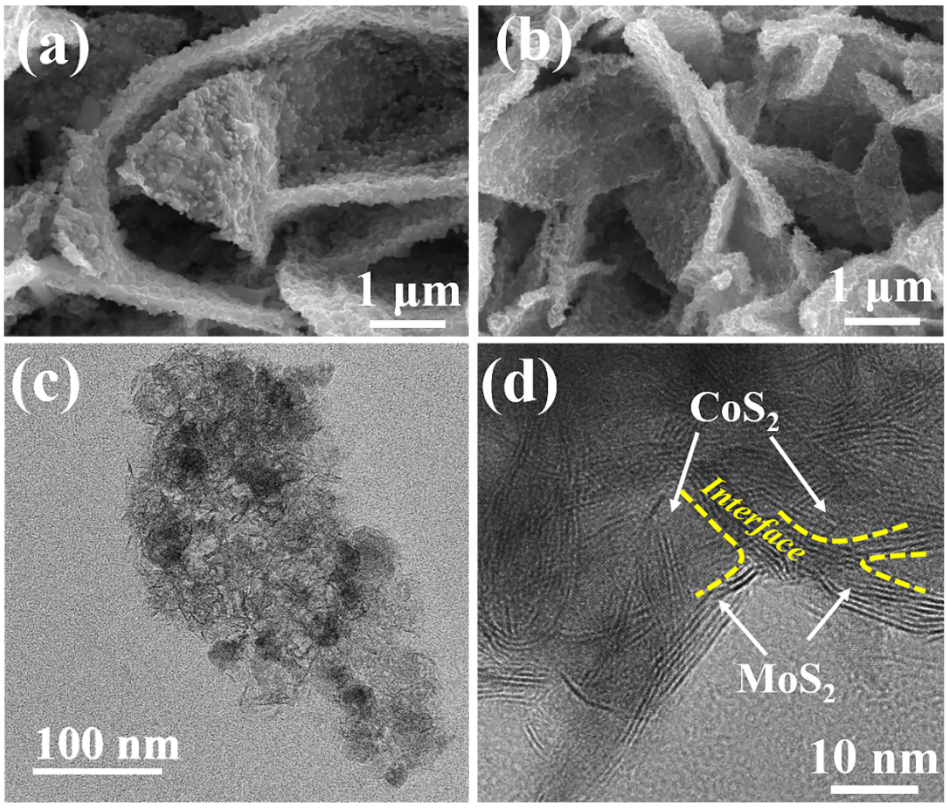

Fig. S4. SEM (a-b), TEM (c), and HRTEM (d) images of 1T-2H MoS_2/CoS_2 heterostructure, where the yellow curves in (d) represent the interface.

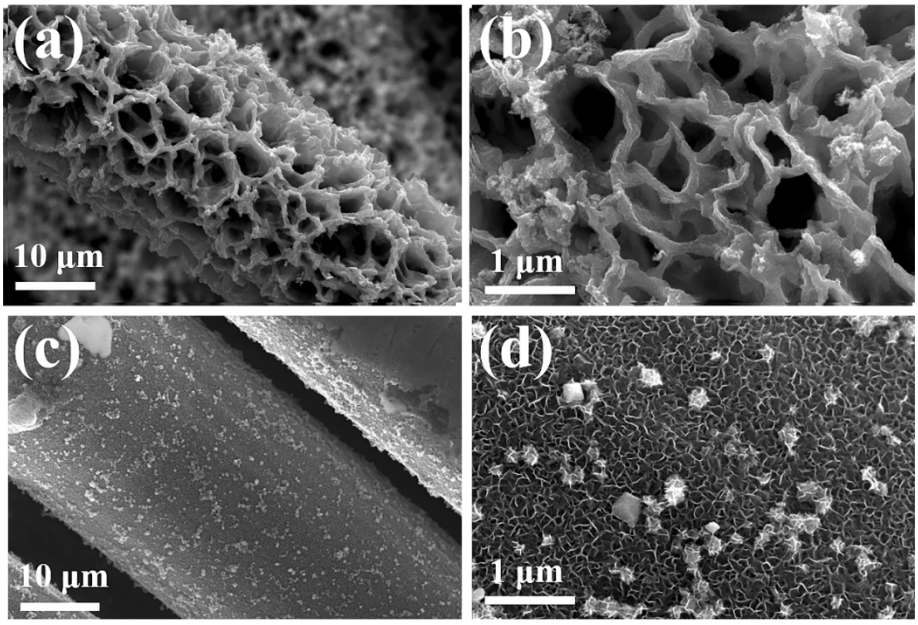

Fig. S5. SEM images of pure CoS_2 (a-b) and MoS_2 (c-d).

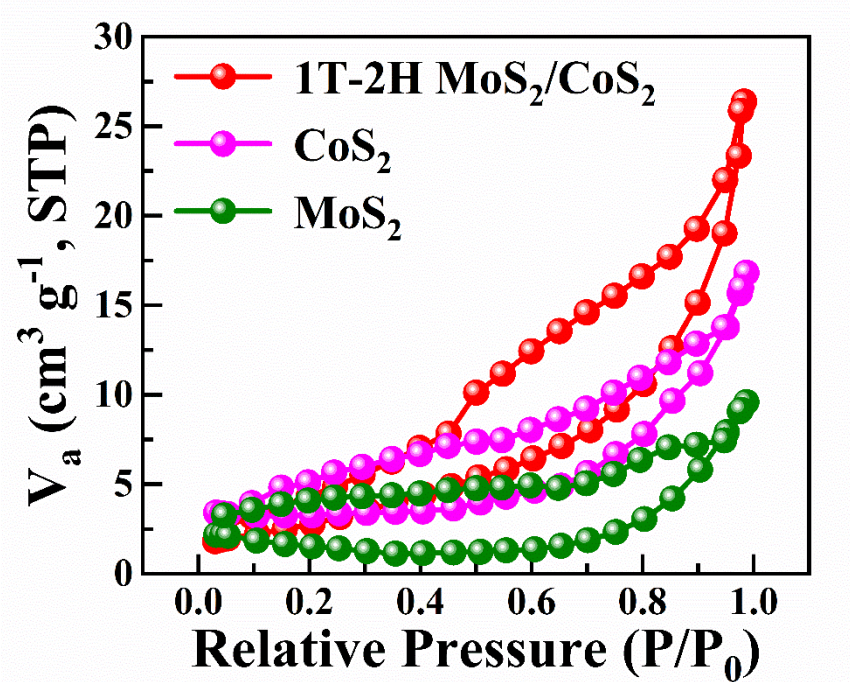

Fig. S6. The BET curves of specific surface area of CoS_2, MoS_2 and 1T-2H MoS_2/CoS_2 heterostructure.

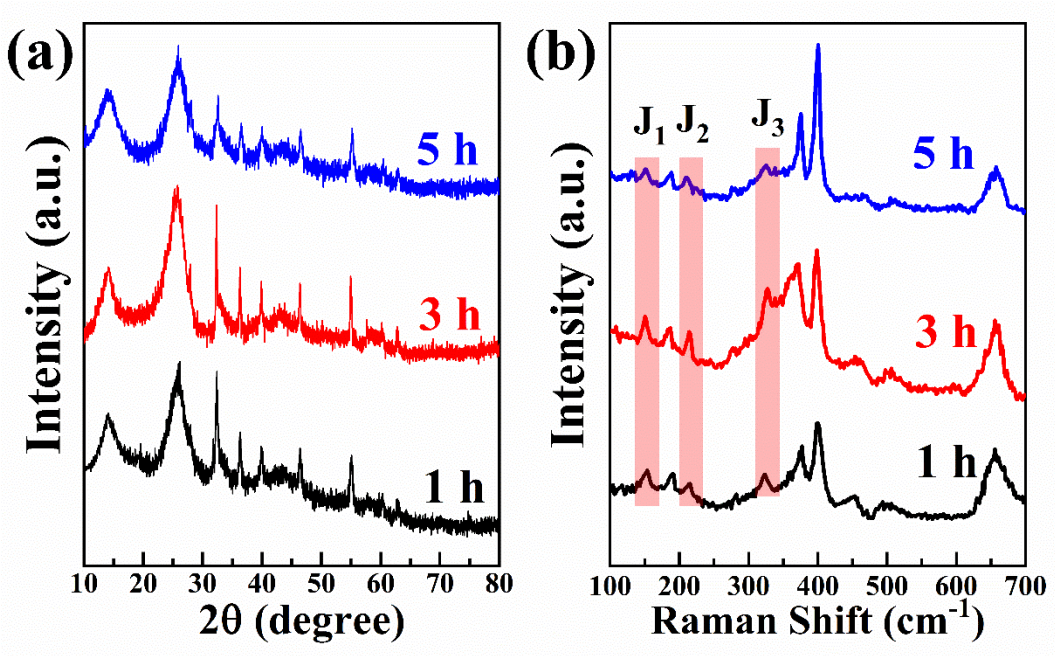

Fig. S7. XRD patterns (a) and Raman spectra (b) of MoS_2/CoS_2-1, MoS_2/CoS_2-3, and MoS_2/CoS_2-5 heterostructures.

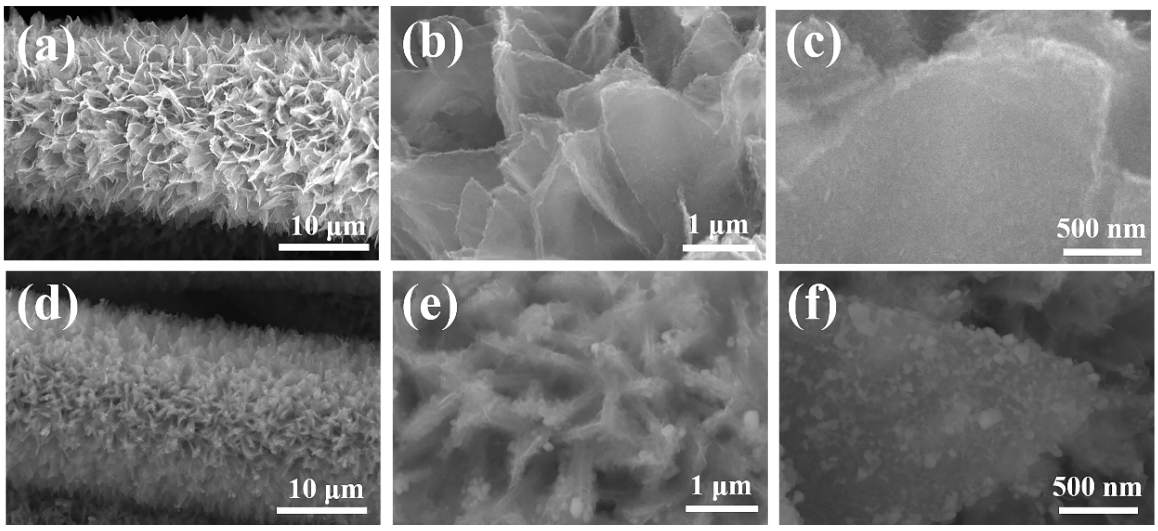

Fig. S8. SEM images of MoS_2/CoS_2-1 (a-c) and MoS_2/CoS_2-5 (d-f) heterostructures.

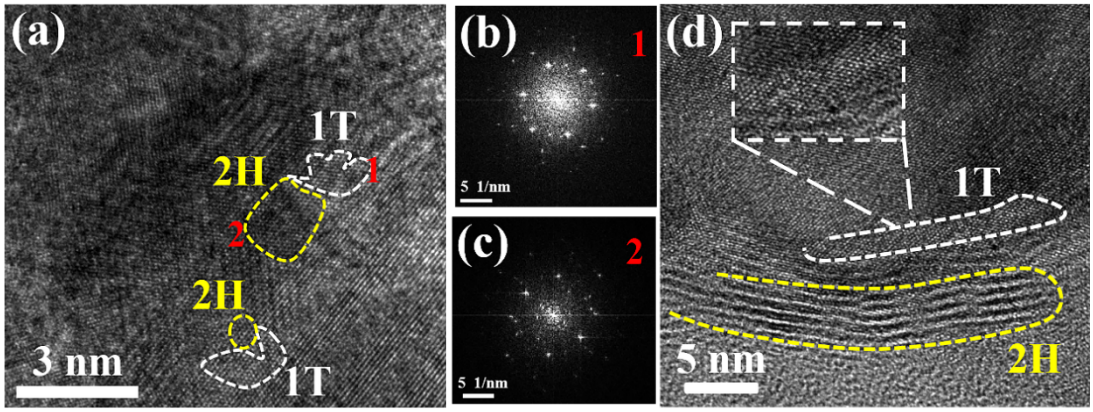

Fig. S9. (a, d) HRTEM images of 1T-2H MoS_2/CoS_2. (b, c) SAED images at positions 1 and 2 in (a), respectively.

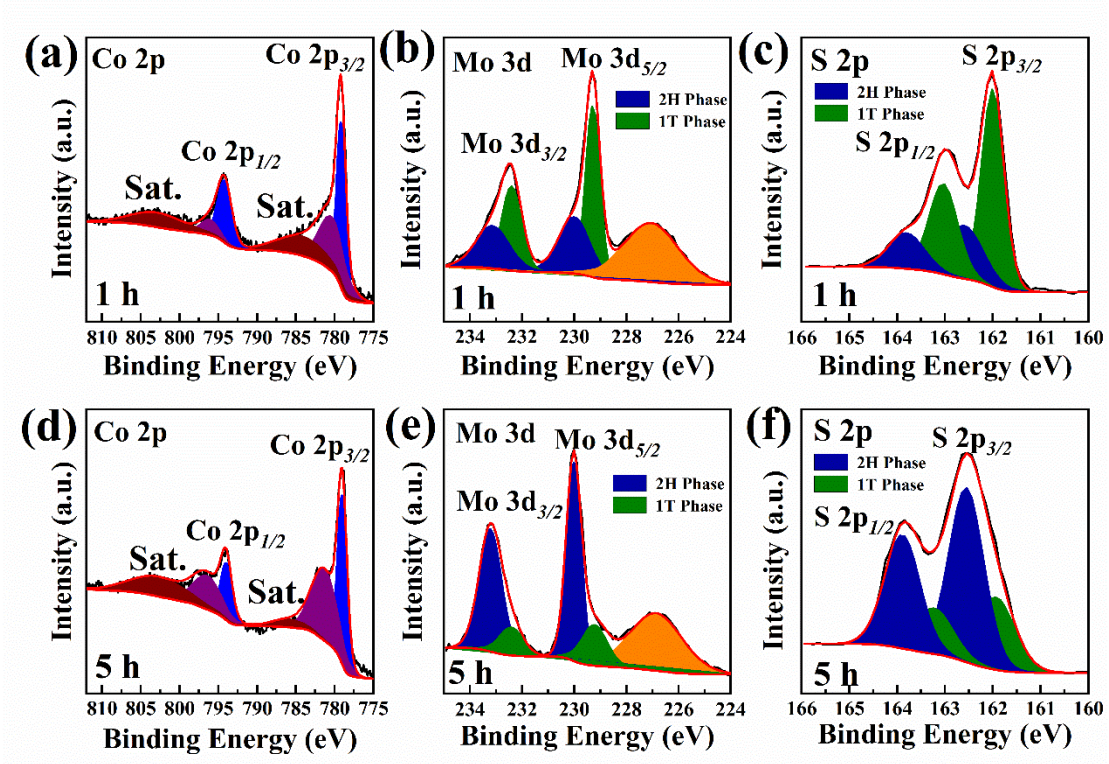

Fig. S10. XPS spectra of Co 2*p*, Mo 3*d*, and S 2*p* for MoS_2/CoS_2-1 (a-c) and MoS_2/CoS_2-5 (d-f), respectively.

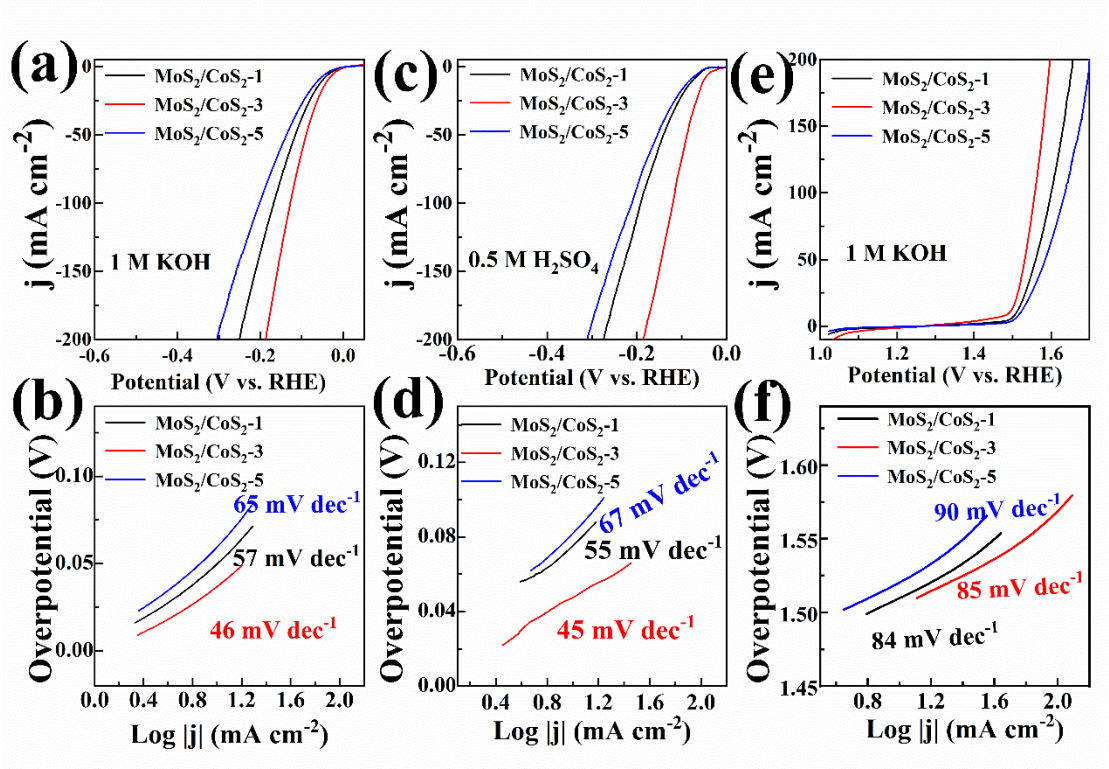

Fig. S11. HER polarization curves (a, c) and the corresponding Tafel slopes (b, d) for MoS_2/CoS_2-1, MoS_2/CoS_2-3 and MoS_2/CoS_2-5 in 1 M KOH and 0.5 M H_2SO_4. (e, f) OER polarization curves and the corresponding Tafel slopes of MoS_2/CoS_2-1, MoS_2/CoS_2-3 and MoS_2/CoS_2-5 in 1 M KOH.

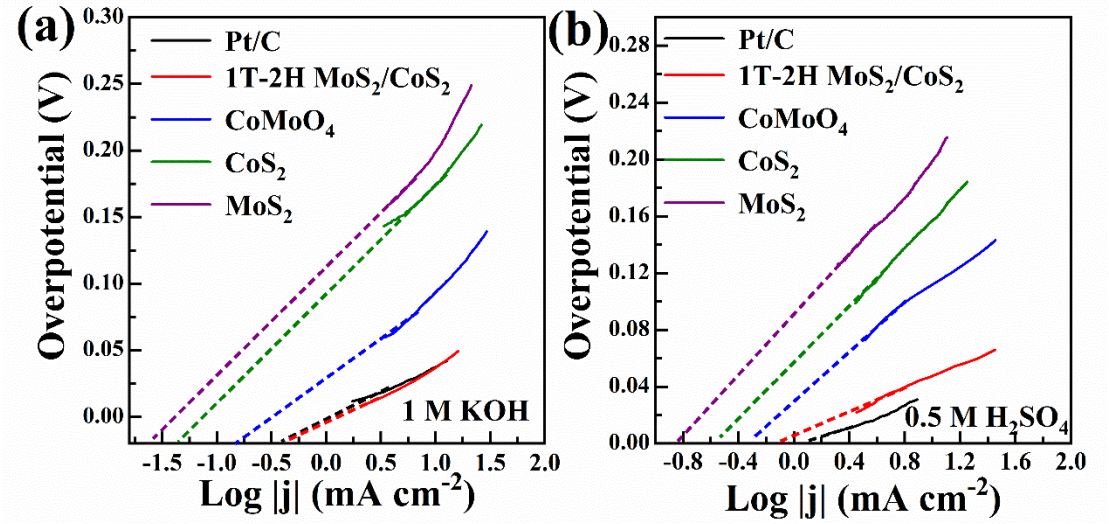

Fig. S12. Calculation of the exchange current densities of Pt/C, 1T-2H MoS_2/CoS_2, $CoMoO_4$, CoS_2, and MoS_2 in 1 M KOH (a) and 0.5 M H_2SO_4 (b).

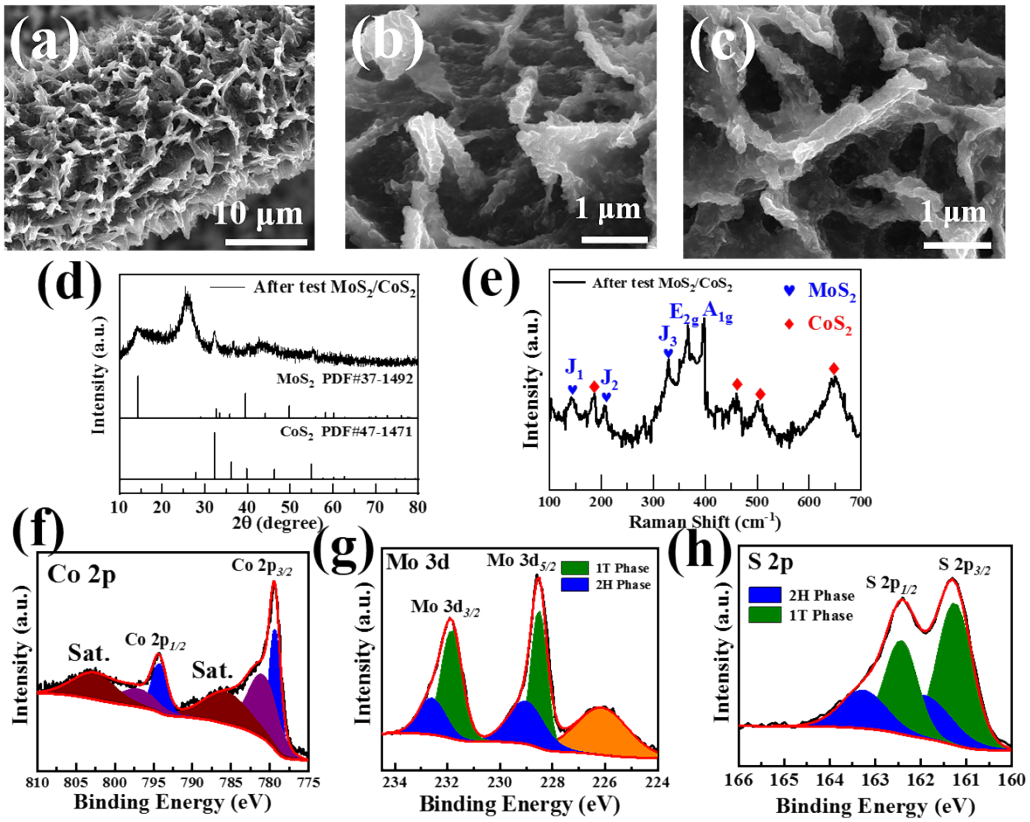

Fig. S13. SEM images (a-c), XRD pattern (d), Raman spectrum (e), and XPS spectra (f-h) of 1T-2H MoS_2/CoS_2 after chronoamperometry test.

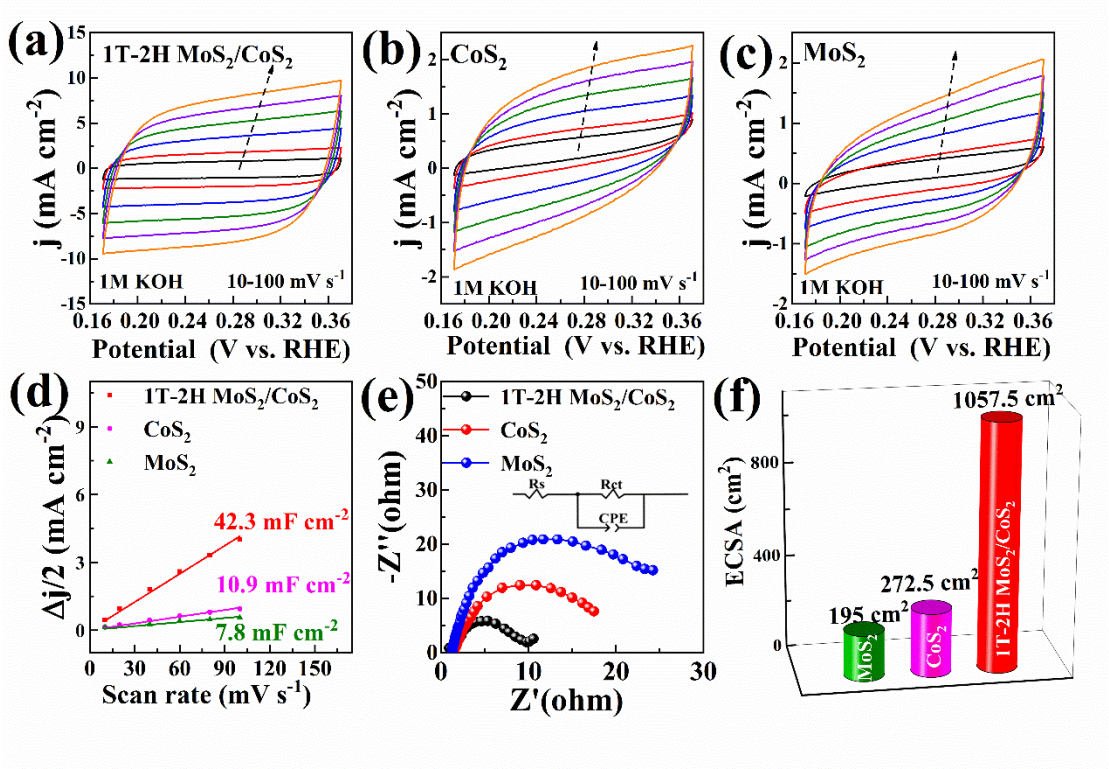

Fig. S14. CV curves in double layer region (0.17-0.37 V *vs*. RHE) (a-c), electrochemical double-layer capacitances (d), Nyquist plots (e), and electrochemical active surface area (f) for 1T-2H MoS_2/CoS_2, CoS_2, and MoS_2 at different scan rates (10~100 mV s^{-1}), respectively. All tests were performed in 1 M KOH.

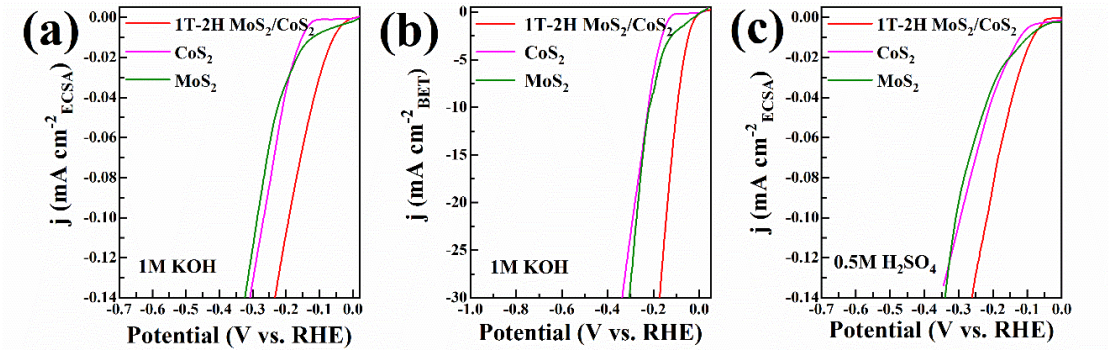

Fig. S15. Specific activities of 1T-2H MoS_2/CoS_2, CoS_2, and MoS_2 in 1 M KOH normalized by ECSA (a) and BET surface area (b), respectively. (c) Specific activities of 1T-2H MoS_2/CoS_2, CoS_2, and MoS_2 at 0.5 M H_2SO_4 normalized by ECSA.

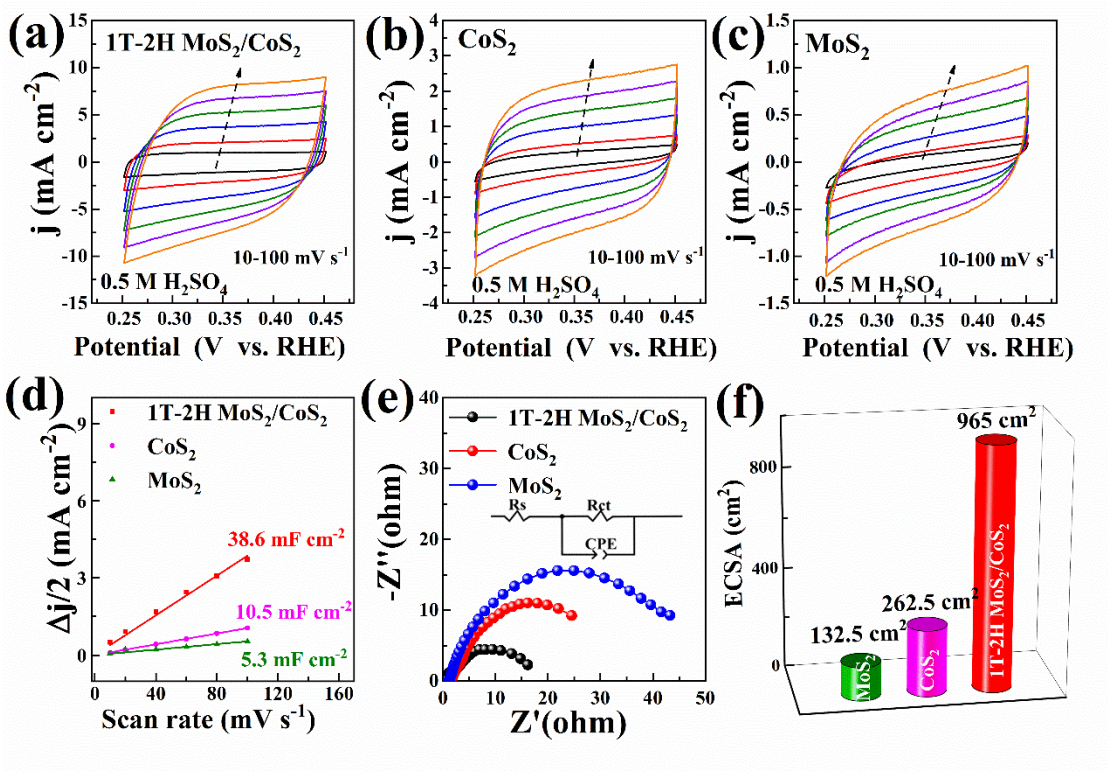

Fig. S16. CV curves in double layer region (0.25-0.45 V *vs*. RHE) (a-c), electrochemical double-layer capacitances (d), Nyquist plots (e), and electrochemical active surface area (f) for 1T-2H MoS_2/CoS_2, CoS_2, and MoS_2 at different scan rates (10~100 mV s^{-1}), respectively. All tests were performed in 0.5 M H_2SO_4.

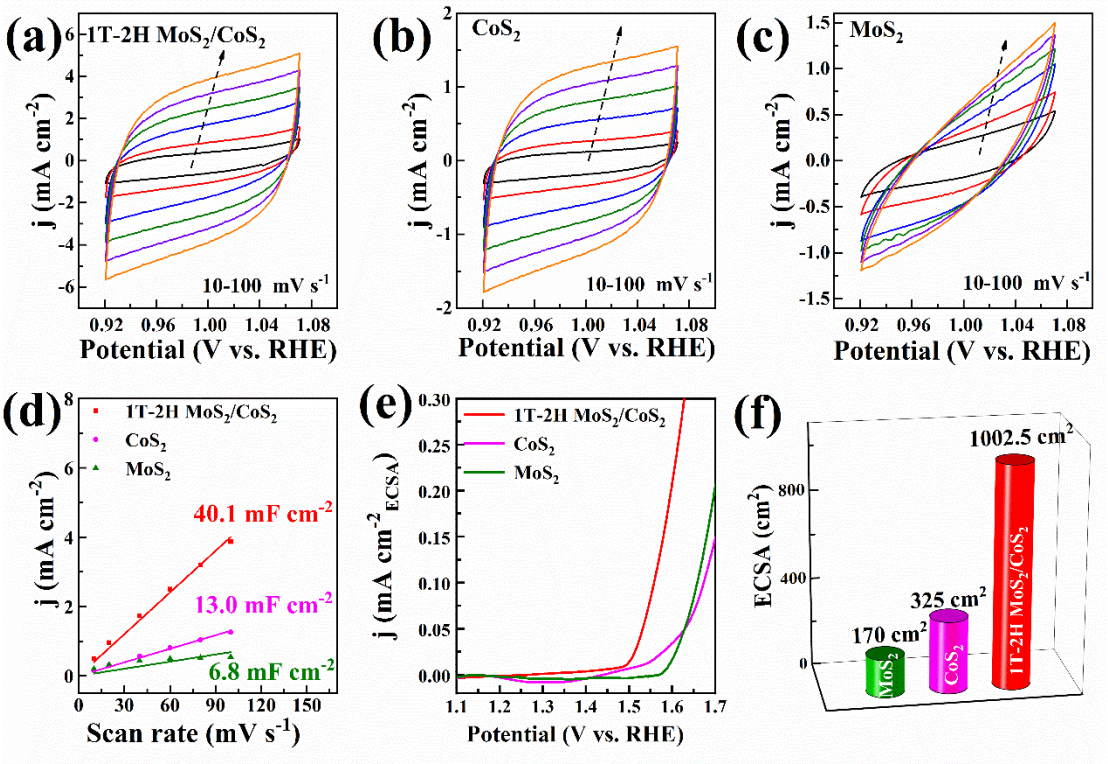

Fig. S17. CV curves in double layer region (0.92-1.07 V vs. RHE) (a-c), electrochemical double-layer capacitances (d), specific activities normalized by ECSA (e), and electrochemical active surface areas (f) for 1T-2H MoS_2/CoS_2, CoS_2, and MoS_2 at different scan rates (10~100 mV s^{-1}), respectively. All tests were performed in 1 M KOH.

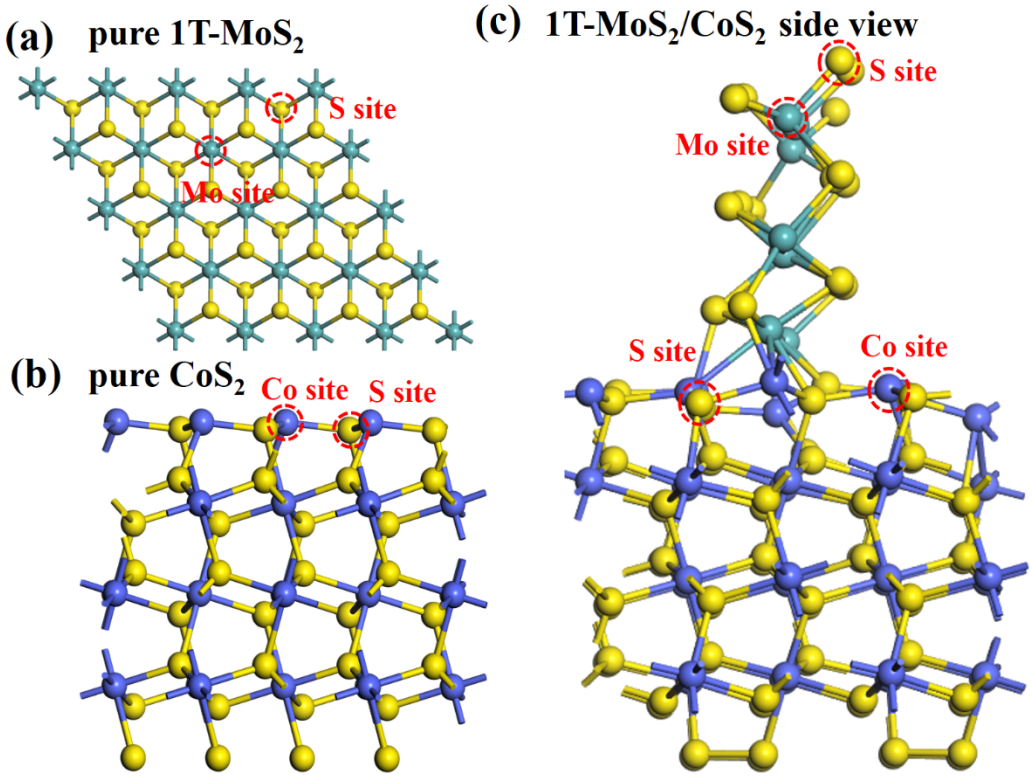

Fig. S18. The H adsorption configurations. (a) The adsorption on Mo and S sites for 1T-MoS_2. (b) The adsorption on Co and S sites for CoS_2(100). The adsorption on Mo, Co and S sites for 1T-MoS_2/CoS_2 heterostructure (c). The cyan, yellow, and light blue balls represent Mo, S, and Co atoms, respectively.

Table S1. The performance of various catalysts for HER in 1 M KOH.

	Loading (mg cm^{-2})	η_{10} (mV)	Tafel slope (mV dec^{-1})	Exchange current j_0 (mA cm^{-2})	TOF value at 150 mV overpotential (s^{-1} per site)
Pt/C	2.01	40	37	1.31	0.091
1T-2H MoS_2/CoS_2	2.03	37	46	1.30	0.070
$CoMoO_4$	1.97	94	78	0.75	0.019
CoS_2	2.05	175	90	0.25	0.003
MoS_2	2.11	200	108	0.18	0.002

Table S2. Comparison of HER performance of 1T-2H MoS_2/CoS_2 with other non-noble metal electrocatalysts in 1 M KOH.

Catalyst	η_{10} (mV)	Tafel slope (mV dec^{-1})	Reference
1T-2H MoS_2/CoS_2	37	46	**This work**
MoS_2-CoS_2 HANs/Ti	82	59	[3]
Co_3O_4/MoS_2	205	98	[4]
$CoS_{1.097}/MoS_2$	249	75	[5]
Mo-Co_9S_8@C	113	67	[6]
1T-MoS_2/CoS_2	71	60	[7]
Ni-MoS_2	98	60	[8]
MoS_2/CoS_2 NTs	85	34	[9]
meso-$FeMoS_2/CoMo_2S_4$	122	90	[10]
$MoS_2/Co_9S_8/Ni_3S_2$	113	85	[11]
NiS–MoS_2 HNSAs/CC	106	56	[12]
NiS_2/MoS_2-CC	91	57	[13]
$MoS_2/Ni_3V_2O_8$	48	46	[14]
MoS_2/NiS_2	68	50	[15]

Table S3. The performance of various catalysts for HER in 0.5 M H_2SO_4.

	η_{10} (mV)	Tafel slope (mV dec^{-1})	Exchange current j_0 (mA cm^{-2})	TOF value at 150 mV overpotential (s^{-1} per site)
Pt/C	36	35	1.30	0.124
1T-2H MoS_2/CoS_2	51	45	0.81	0.040
$CoMoO_4$	112	75	0.35	0.020
CoS_2	156	91	0.28	0.005
MoS_2	208	105	0.16	0.003

Table S4. Comparison of HER performance of 1T-2H MoS_2/CoS_2 with other non-noble metal electrocatalysts in 0.5 M H_2SO_4.

Catalyst	η_{10} (mV)	Tafel slope (mV dec^{-1})	Reference
1T-2H MoS_2/CoS_2	51	45	**This work**
CoS_2@1T-MoS_2	72	45	[16]
1T-MoS_2/CoS_2	26	43	[7]
$CoS_{1.097}/MoS_2$	228	59	[5]
1T/2H MoS_2	131	106	[17]
MoS_2-CoS_2@PCMT	200	95	[18]
Mo-Co_9S_8@C	98	34	[6]
MoP/MoS_2@CC	69	61	[19]
$MoS_2/Co_9S_8/Ni_3S_2$/NF	103	55	[20]
CoP/NiCoP/NC	60	78	[21]
MoNiCNTs	182	49	[22]

Table S5. The performance of various catalysts for OER and overall water splitting in 1 M KOH.

	η_{10} (mV)	Tafel slope (mV dec^{-1})	TOF value at 400 mV overpotential (s^{-1} per site)	η_{10} (V) cell voltage
IrO_2	233	82	0.063	1.52
1T-2H MoS_2/CoS_2	261	85	0.080	1.53
$CoMoO_4$	335	102	0.012	1.67
CoS_2	363	123	0.006	1.68
MoS_2	405	142	0.002	1.76

Table S6. Comparison of OER performance of 1T-2H MoS_2/CoS_2 with other non-noble metal electrocatalysts in 1 M KOH.

Catalyst	η_{10} (mV)	Tafel slope (mV dec^{-1})	Reference
1T-2H MoS_2/CoS_2	261	85	**This work**
MoS_2-CoS_2 HANs/Ti	266	104	[3]
meso-$FeMoS_2/CoMo_2S_4$	290	65	[10]
$MoS_2/Co_9S_8/Ni_3S_2$	166	58	[11]
MoS_2/NiCoS	290	77	[23]
MoS_2/Ni_3S_2	278	91	[24]
Co_3O_4/MoS_2	230	45	[4]
Co_3S_4@MoS_2	280	43	[25]
NiS–MoS_2 HNSAs/CC	203	77	[26]
NiS-Ni_3S_2/NF	269	119	[27]
NiS_2/MoS_2-CC	362	117	[13]
MoS_2/NiS	278	91	[15]

Table S7. Comparison of overall water splitting performance of 1T-2H MoS_2/CoS_2 with other non-noble metal electrocatalysts in 1 M KOH.

Catalyst	η_{10} (V) Cell voltage	Reference
1T-2H MoS_2/CoS_2	1.53	**This work**
Mo-Co_9S_8@C	1.56	[6]
NiS–MoS_2 HNSAs/CC	1.54	[26]
$MoS_2/Ni_3V_2O_8$	1.58	[14]
MoS_2/NiS_2	1.59	[24]
N-CoS_2/G	1.58	[28]
N-Ni_3S_2/CoS_2/NF	1.56	[29]
MoS_2/NiCoS	1.50	[23]
Ni_2P-MoS_2 HNSAs/CC	1.57	[30]
MoS_2@CoNi-ZIF	1.55	[31]

References:

1. M. Gong, Y. Li, H. Wang, Y. Liang, J. Z. Wu, J. Zhou, J. Wang, T. Regier, F. Wei and H. Dai, *J. Am. Chem. Soc.*, 2013, **135**, 8452-8455.
2. J. Xu, J. Li, D. Xiong, B. Zhang, Y. Liu, K.-H. Wu, I. Amorim, W. Li and L. Liu, *Chem. Sci.*, 2018, **9**, 3470-3476.
3. Y. Li, W. Wang, B. Huang, Z. Mao, R. Wang, B. He, Y. Gong and H. Wang, *J. Energy Chem.*, 2021, **57**, 99-108.
4. A. Muthurasu, V. Maruthapandian and H. Y. Kim, *Appl. Catal. B*, 2019, **248**, 202-210.
5. J. Sun, Z. Huang, T. Huang, X. Wang, X. Wang, P. Yu, C. Zong, F. Dai and D. Sun, *ACS Appl. Energy Mater.*, 2019, **2**, 7504-7511.
6. L. Wang, X. Duan, X. Liu, J. Gu, R. Si, Y. Qiu, Y. Qiu, D. Shi, F. Chen and X. Sun, *Adv. Energy Mater.*, 2020, **10**, 1903137.
7. Y. Feng, T. Zhang, J. Zhang, H. Fan, C. He and J. Song, *Small*, 2020, **16**, 2002850.
8. C. Lei, Y. Wang, Y. Hou, P. Liu, J. Yang, T. Zhang, X. Zhuang, M. Chen, B. Yang and L. Lei, *Energy Environ. Sci.*, 2019, **12**, 149-156.
9. B. Tang, Z. G. Yu, Y. Zhang, C. Tang, H. L. Seng, Z. W. Seh, Y.-W. Zhang, S. J. Pennycook, H. Gong and W. Yang, *J. Mater. Chem. A*, 2019, **7**, 13339-13346.
10. Y. Guo, J. Tang, J. Henzie, B. Jiang, W. Xia, T. Chen, Y. Bando, Y.-M. Kang, M. S. A. Hossain and Y. Sugahara, *ACS Nano*, 2020, **14**, 4141-4152.
11. Y. Yang, H. Yao, Z. Yu, S. M. Islam, H. He, M. Yuan, Y. Yue, K. Xu, W. Hao, G. Sun, H. Li, S. Ma, P. Zapol and M. G. Kanatzidis, *J. Am. Chem. Soc.*, 2019, **141**, 10417-10430.
12. S. Guan, X. Fu, Z. Lao, C. Jin and Z. Peng, *Sustain. Energy Fuels*, 2019, **3**, 2056-2066.
13. X. Wang, L. Li, Z. Wang, L. Tan, Z. Wu, Z. Liu, S. Gai and P. Yang, *Electrochim. Acta*, 2019, **326**, 134983.
14. P. Chang, S. Zhang, X. Xu, Y. Lin, X. Chen, L. Guan and J. Tao, *Chem. Eng. J.*, 2021, **423**, 130196.
15. S. Ye, F. Luo, Q. Zhang, P. Zhang, T. Xu, Q. Wang, D. He, L. Guo, Y. Zhang, C. He, X. Ouyang, M. Gu, J. Liu and X. Sun, *Energy Environ. Sci.*, 2019, **12**, 1000-1007.
16. Z. Liu, K. Wang, Y. Li, S. Yuan, G. Huang, X. Li and N. Li, *Appl. Catal. B*, 2022, **300**, 120696.
17. K. Le, X. Zhang, Q. Zhao, Y. Liu, P. Yi, S. Xu and W. Liu, *ACS Appl. Mater. Interface.*, 2021, **13**, 44427-44439.
18. M. Liu, H. N. Jaiswal, S. Shahi, S. Wei, Y. Fu, C. Chang, A. Chakravarty, X. Liu, C. Yang, Y. Liu, Y. H. Lee, V. Perebeinos, F. Yao and H. Li, *ACS Nano*, 2021, **15**, 5762-5772.
19. A. Wu, Y. Gu, Y. Xie, C. Tian, H. Yan, D. Wang, X. Zhang, Z. Cai and H. Fu, *ACS Appl. Mater. Interface.*, 2019, **11**, 25986-25995.
20. Y. Yang, H. Yao, Z. Yu, S. M. Islam, H. He, M. Yuan, Y. Yue, K. Xu, W. Hao

and G. Sun, *J. Am. Chem. Soc.*, 2019, **141**, 10417-10430.
21. R. Boppella, J. Tan, W. Yang and J. Moon, *Adv. Funct. Mater.*, 2019, **29**, 1807976.
22. X. Zhang and P. Yang, *Carbon*, 2021, **175**, 176-186.
23. C. Qin, A. Fan, X. Zhang, S. Wang, X. Yuan and X. Dai, *J. Mater. Chem. A*, 2019, **7**, 27594-27602.
24. J. Lin, P. Wang, H. Wang, C. Li, X. Si, J. Qi, J. Cao, Z. Zhong, W. Fei and J. Feng, *Adv. Sci.*, 2019, **6**, 1900246.
25. Y. Guo, J. Tang, Z. Wang, Y.-M. Kang, Y. Bando and Y. Yamauchi, *Nano Energy*, 2018, **47**, 494-502.
26. S. Guan, X. Fu, Z. Lao, C. Jin and Z. Peng, *Sustain. Energy Fuels*, 2019, **3**, 2056-2066.
27. J. Wang and H. C. Zeng, *ACS Appl. Mater. Interface.*, 2019, **11**, 23180-23191.
28. Y. Tong, Q. Sun, P. Chen, L. Chen, Z. Fei and P. J. Dyson, *ChemSusChem*, 2020, **13**, 5112-5118.
29. Q. Kong, N. Fan, S. Chen, X. Wu, L. Liu, R. Lang, Z. Gao, H. Guan, C. Dong and G. Chen, *J. Electroanal. Chem.*, 2021, **895**, 115516.
30. B. Zhang, K. Xu, X. Fu, S. Guan, X. Li and Z. Peng, *J. Alloy. Compd.*, 2021, **856**, 158094.
31. Y. Liu, B. Hu, S. Wu, M. Wang, Z. Zhang, B. Cui, L. He and M. Du, *Appl. Catal. B*, 2019, **258**, 117970.